Triad resonant instability of horizontally periodic internal modes

Bruce R. Sutherland [1,2,*] and Riley Jefferson [1]
[1]*Department of Physics, University of Alberta, Edmonton, Alberta, Canada T6G 2E1*
[2]*Department of Earth & Atmospheric Sciences, University of Alberta, Edmonton, Alberta, Canada T6G 2E3*

(Received 11 September 2019; accepted 14 February 2020; published 19 March 2020)

Theory is developed to predict the growth and structure of "sibling" waves developing through triadic resonant instability of a vertically confined mode-1 internal "parent" wave in uniform stratification including the influence of background rotation. For a sufficiently hydrostatic parent wave, two branches for growth of sibling waves are dominant. The branch with largest growth rate corresponds to sibling waves having frequencies much larger than that of the parent; the other branch corresponds to sibling waves having frequencies close to half the frequency of the parent. Numerical simulations show that sibling waves corresponding to the subharmonic branch appear in practice. In the absence of rotation, the sibling waves corresponding to this branch are predicted to have near-constant growth rate as their horizontal wave number increases. With rotation, however, the growth rate peaks at moderate wave number. In all cases, as confirmed by numerical simulations, the e-folding time for the growth of the sibling waves can be thousands of buoyancy periods for parent waves having amplitudes typical of realistic oceanic internal modes. In nonuniform stratification, the parent wave self-interacts immediately to force superharmonics. Nonetheless, numerical simulations with symmetric top-hat stratification show that triadic resonant instability eventually emerges. Such emergence is not evident in simulations with stratification more representative of the ocean. The results suggest a reconsideration of the efficacy of parametric subharmonic instability in leading to the breakdown of low-mode internal tides in the ocean.

DOI: 10.1103/PhysRevFluids.5.034801

I. INTRODUCTION

It is estimated that globally 1 TW of power is transferred from the lunisolar tides to internal tides [1]. The action of the barotropic tide over bottom topography can generate vertically propagating beams near the source. While some fraction of that energy is dissipated in the near field (as observed, for example, near the Hawaiian Ridge [2]), most of the energy becomes manifest as low-mode internal tides in the far field where they may then propagate thousands of kilometers from the source [3]. An outstanding question asks how the energy from these waves ultimately cascades from large to small scale where it may be dissipated, thus closing this branch of the oceanic energy budget. Several possibilities have been explored, including dissipation when the internal tide interacts with rough bottom topography, with the continental slopes and shelves, and with mean flows and eddies (for a recent review, see MacKinnon *et al.* [4]). It has also been suggested that, away from topography and background flows, internal modes may be dissipated due to nonlinear wave-wave interactions including the case of triadic resonant instability (hereafter TRI), in which a pair of "sibling" waves grow out of the background noise field through resonant interactions with the "parent" wave (for a

*bruce.sutherland@ualberta.ca

recent review, see Dauxois *et al.* [5]). TRI is more general than parametric subharmonic instability (PSI), in which the sibling waves are both restricted to have lower frequency than the parent (and, typically, each has half the parent wave frequency). That said, TRI is a special case of "resonant triad interactions" [6], in which the three interacting waves can have comparable amplitude. Here our theoretical focus is on the growth of sibling waves when their amplitude remains small compared to the parent. Indirect evidence for the occurrence of TRI has been inferred from observations of enhanced dissipation equatorward of about 30° latitude [7,8]. It has been proposed that within this latitude band about the equator the dominant M_2 internal tide becomes unstable to subharmonics with nearly half the M_2 tidal frequency. Because these subharmonics have the same frequency as the Coriolis frequency at 28.9° latitude, they are predicted to pile up and break near this critical latitude. Although the hypothesis was verified in idealized numerical simulations [9,10], *in situ* observations around 29°N close to Hawaii did not reveal a particularly strong "subtropical catastrophe," although some evidence for the occurrence of subharmonic resonance was inferred through the examination of bispectra [11]. Inspired by these observations, high-resolution ocean general circulation models have been performed and analyzed with bispectral analyses to assess the occurrence of TRI in the global oceans [12]. In an idealized numerical study of internal modes in uniform stratification lying in the latitude band between 28°S and 28°N, TRI for sibling waves with half the internal tide frequency was found to transfer energy at a rate approximately half of that presently assumed to be input through barotropic to baroclinic energy conversion [13].

Strictly speaking, the theory for TRI considers the interaction of a pair of "sibling" waves with a "parent" wave in vertically and horizontally unbounded uniformly stratified fluid. In this case, each monochromatic wave has a well defined frequency and wave number vector corresponding to sinusoidal waves [5]. It is expected that a bounded internal mode in uniform stratification should likewise be susceptible to TRI since the vertical structure can be viewed as a superposition of two oppositely propagating phase-locked sinusoidal waves. Indeed, this has been observed in laboratory experiments in which a mode 1-1 internal wave was excited in a tank with square vertical cross section by vertically oscillating the tank at the predicted frequency of this mode [14,15]. Notably, the growth of the instability was most pronounced in the center of the tank, whereas no such spatial localization occurs for TRI developing from an unbounded plane wave. TRI has also been observed to develop in a laboratory experiment in which a horizontally propagating, vertically bounded mode-1 wave was generated at one end of a tank filled with uniformly stratified fluid [16]. After a time corresponding to about 30 periods of the highly nonhydrostatic parent mode, sibling waves were observed to develop as sets of upward and downward propagating beams emanating most strongly at middepth near the wave generator.

It is unclear how the theory for TRI can rigorously be extended to the case more representative of low-mode internal tides in the ocean that propagate horizontally through nonuniform stratification. Key to the theory leading to the wave number and frequency triadic resonance conditions is that the parent and sibling waves are sinusoidal both vertically and horizontally. Thus one sinusoidal wave interacts with a second sinusoidal wave through the advective terms in the equations of motion to create a third sinusoidal wave. However, internal modes in nonuniform stratification do not have sinusoidal vertical structure. Furthermore, such modes are known to self-interact through the advective terms so as to provide superharmonic forcing to the medium [17–20]. In applying the theory for TRI to internal waves in nonuniform stratification, a typical assumption is that the resonantly excited sibling waves have such small vertical scale that they develop through interaction with the parent mode over a relatively small vertical depth, presumably where the vertical structure of the stream function of the parent mode is largest and so partially map onto a sinusoidal disturbance. In the special case of a parent wave having double the background Coriolis frequency, Young *et al.* [21] predicted that subharmonic near-inertial sibling waves should grow through parametric subharmonic instability. Here our intent is to examine TRI for parent waves spanning the range from nonhydrostatic (as in laboratory experiments) to hydrostatic (as in the ocean) and, aided by numerical simulations, examine the influence of the vertical confinement of the parent mode upon the occurrence of TRI.

The general theory for TRI including the influence of Coriolis forces is reviewed in Sec. II, wherein predictions for the structure and frequency of sibling waves in uniform stratification are provided. The setup of the numerical model is described in Sec. III with the results for uniform stratification presented in Sec. IV and results for nonuniform stratification discussed in Sec. V. The interpretation of these results for understanding the occurrence of TRI from internal tides in the ocean is discussed in Sec. VI.

II. THEORY

We consider triadic resonant instabilities associated with horizontally periodic two-dimensional internal waves on the f-plane in a domain of uniform depth H bounded above and below by free-slip boundaries. With the intent to model the evolution of oceanic internal tides, the effects of diffusion and viscosity are neglected. As such this work is an extension of the theory of Bourget *et al.* [22] who neglected the Coriolis parameter, f, but included viscosity to aid in the interpretation of laboratory experiments, and of the work of Young *et al.* [21] who focused upon parametric subharmonic instability for sibling waves having frequencies near f.

A. Fully nonlinear equations of motion

Neglecting viscosity and diffusion, the fully nonlinear equations of motion confined to the x-z plane for an incompressible, rotating, Boussinesq fluid on the f plane are

$$\partial_t u + \partial_x(uu) + \partial_z(wu) - fv = -\partial_x p/\rho_0, \tag{1a}$$

$$\partial_t v + \partial_x(uv) + \partial_z(wv) + fu = 0, \tag{1b}$$

$$\partial_t w + \partial_x(uw) + \partial_z(ww) = -\partial_z p/\rho_0 + b, \tag{1c}$$

$$\partial_t b + \partial_x(ub) + \partial_z(wb) = -N^2 w, \tag{1d}$$

$$\partial_x u + \partial_z w = 0, \tag{1e}$$

in which $b = -g\rho/\rho_0$ is the buoyancy, (u, v, w) is the velocity vector with components respectively in the x, y, and z directions, ρ and p are, respectively, the fluctuation density and pressure, g is gravity, ρ_0 is the characteristic density, f is the (constant) Coriolis parameter, and $N^2 = -(g/\rho_0)d\bar{\rho}/dz$ is the squared buoyancy frequency expressed in terms of the vertical gradient of the background density $\bar{\rho}$. In writing these equations, the x axis is aligned with the horizontal phase velocity of the parent wave and it is assumed that the spanwise extent of the wave is so wide that it can be considered to be y-independent. As follows from (1e), the velocity in the x-z plane can be defined in terms of the stream function ψ, so that $(u, w) = (-\partial_z\psi,\ \partial_x\psi)$.

Taking the curl of (1a) and (1c) to formulate the equation for the evolution of the spanwise vorticity and using (1b) and (1d) gives the following equation written as a linear operator L acting on ψ forced by nonlinear terms $\mathcal{N}$:

$$\underbrace{[\partial_{tt}(\partial_{xx} + \partial_{zz}) + N^2\partial_{xx} + f^2\partial_{zz}]}_{\equiv L}\,\psi = \underbrace{\vec{\nabla}\cdot[\partial_t(\vec{u}\zeta) - \partial_x(\vec{u}b) + f\partial_z(\vec{u}v)]}_{\equiv N}, \tag{2}$$

in which $\zeta = \partial_z u - \partial_x w$ is the spanwise vorticity, $\vec{\nabla} = (\partial_x, \partial_z)$ and $\vec{u} = (u, w)$.

B. Small-amplitude internal modes

For small-amplitude waves with horizontal (in x) wave number k and frequency ω, the nonlinear terms on the right-hand side of (2) can be neglected, yielding a linear differential eigenvalue equation whose solution gives the vertical structure, Ψ, of the stream function as it depends upon $N^2(z)$

together with the corresponding dispersion relation $\omega = \omega(k)$. Explicitly, for given k, Ψ satisfies

$$\Psi'' + k^2 \frac{N^2(z) - \omega^2}{\omega^2 - f^2}\Psi = 0. \tag{3}$$

In the case of uniform stratification ($N = N_0$ constant) for vertically bounded waves in a domain of depth H, such internal modes with horizontal wave number $k = k_0$ are given by

$$\psi_0(x, z, t) = \tfrac{1}{2} a_0 \sin(m_0 z) \exp[\imath(k_0 x - \omega_0 t)] + \text{c.c.} \tag{4}$$

in which c.c. represents the complex conjugate, a_0 is the stream function amplitude, $m_0 = \pi/H$ is the vertical wave number of the lowest internal mode and the dispersion relation is

$$\omega_0 = \sqrt{\frac{N_0^2 k_0^2 + f^2 m_0^2}{k_0^2 + m_0^2}}. \tag{5}$$

Of course one can write $\sin(m_0 z) = -(\imath/2)[\exp(\imath m_0 z) - \exp(-\imath m_0 z)]$. As such, ψ_0 in Eq. (4) can be considered as the superposition of two vertically phase-locked plane-periodic waves.

C. Resonant triads

Here we take the traditional view of triadic resonant instability (TRI) that, from a given a "parent wave" of known frequency ω_0, two "sibling waves" with frequencies $\omega_\pm$ can grow out of a background noise field through resonant interactions with the parent, provided the sum of the sibling frequencies equals the parent wave frequency. (In the special case of parametric subharmonic instability, the sibling waves have frequencies $\omega_+ = \omega_- = \omega_0/2$.) Our approach thus differs from studies that have examined the self-interaction of a parent mode resulting in the creation of superharmonics [18–20,23] and mean flow disturbances [20,24]. Furthermore, rather than consider the vertical structure of the stream function given by the solution of (4), we approximate the parent mode structure as being locally sinusoidal where the structure function is near its maximum. We then predict the growth rate of various resonant triads following the approach of Bourget *et al.* [22] (see also Dauxois *et al.* [5]), but including rotation and neglecting viscosity.

In the consideration of TRI of internal modes in uniform stratification, the parent wave with stream function given by (4) has well-defined wave number (k_0, m_0) and frequency ω_0. Superimposed on this mode are pairs of vertically propagating waves having wave numbers $(k_\pm, m_\pm)$ and corresponding frequencies $\omega_\pm$. For this ansatz to hold, $m_\pm$ must necessarily be larger than that of the lowest vertical mode, $m_0 = \pi/H$, to ensure at least a half vertical wavelength fits in the domain. Crucial to this assumption is that the resonantly excited waves extract their energy from the parent wave far from the upper and lower boundaries where the stream function amplitude, $\propto \sin(m_0 z)$, is largest, consistent with experiments [16] and the simulations [9,10]. Hence the presence of the upper and lower boundaries play no role in their excitation, although the consequent vertical propagation of these waves, which reflect from the boundaries, may be influenced by the boundaries in that the reflected waves interfere constructively or destructively with the waves being excited within the domain.

In nonuniform stratification, the parent wave frequency and horizontal wave number are prescribed and the vertical wave number, m_0, is given by inverting (5) in which N_0 is taken to be the buoyancy frequency where the vertical structure of the stream function is largest. Under the assumption that $m_\pm$ is large, the buoyancy frequency about the depth where the sibling waves are strongly excited can be considered as approximately constant: $N \simeq N_0$. The sibling waves can then be represented by

$$\psi_\pm(x, z, t) = \tfrac{1}{2} a_\pm \exp[\imath(k_\pm x + m_\pm z - \omega_\pm t)] + \text{c.c.}, \tag{6}$$

in which

$$\omega_\pm = \sqrt{\frac{N_0^2 k_\pm^2 + f^2 m_\pm^2}{k_\pm^2 + m_\pm^2}}. \tag{7}$$

In these expressions, and below, the subscript sign convention is that the equation holds taking either the upper signs or the lower signs on both sides of the equation. Resonant triads involve the interaction between sibling waves given by (6) and the parent wave such that energy from the parent wave is funneled into the sibling waves. For resonance to occur, the wave numbers and frequencies must satisfy the following resonant triad conditions [5]:

$$k_+ \pm k_- = k_0, \tag{8a}$$

$$m_+ \pm m_- = m_0, \tag{8b}$$

$$\omega_+ \pm \omega_- = \omega_0. \tag{8c}$$

Together with the dispersion relation for ω_0 and $\omega_\pm$, this constitutes an implicit equation for m_+ in terms of some k_+ for given k_0, m_0 and corresponding ω_0. As shown in the Appendix, the result can be recast as the root of a polynomial in $m_+(k_+)$ of degree 8 from whose (real) roots one can then determine $m_-(k_+)$, $k_-(k_+)$ and the corresponding values of $\omega_\pm(k_+)$.

D. Triadic resonant instability

Equation (2) is used to determine how one of the sibling waves grows in time due to the interaction between the other sibling wave and the parent wave through derivation of evolution equations for $a_\pm(t)$. In doing so, it is assumed the growth rate is small so that second time-derivatives on the left-hand side of (2) can be neglected in comparison with first time derivatives of $a_\pm$. Likewise, time derivatives on the right-hand side of (2) acting on $\exp(-\imath\omega_\pm t)$ are assumed to be much larger than time derivatives acting upon the amplitudes a_0 and $a_\pm$.

Thus, after some algebra, we find

$$\dot{a}_\pm = I_\pm \, m_0 k_0 a_0 \, a_\mp^\star \tag{9}$$

in which $\dot{a}_\pm$ represents the time-derivative of $a_\pm$, and $a_\mp^\star$ is the complex conjugate of $a_\mp$. In this expression we have defined the nondimensional quantity $I_\pm$ to be

$$I_\pm = \frac{1}{8}\frac{m_\mp/m_0 - k_\mp/k_0}{\kappa_\pm^2 \omega_\pm}\left\{\omega_\pm(\chi_0 - \chi_\mp) + N_0^2 k_\pm\left(\frac{k_0}{\omega_0} - \frac{k_\mp}{\omega_\mp}\right) + \imath f^2 m_\pm\left(\frac{m_0}{\omega_0} + \frac{m_\mp}{\omega_\mp}\right)\right\}, \tag{10}$$

in which $\kappa_\pm = (k_\pm^2 + m_\pm^2)^{1/2}$ and

$$\chi_\pm = \left(\frac{N_0^2 - f^2}{\omega_\pm^2 - f^2}\right) k_\pm^2. \tag{11}$$

In the special case with $f = 0$, these expressions reduce to those of Bourget *et al.* [22] by neglecting viscosity in their result.

The time evolution separately of a_+ or a_- is thus given by

$$\ddot{a}_+ = I_+ I_-^\star \, m_0^2 k_0^2 |a_0|^2 \, a_+, \quad \ddot{a}_- = I_- I_+^\star \, m_0^2 k_0^2 |a_0|^2 \, a_-. \tag{12}$$

If $f \neq 0$, $I_\pm$ is possibly complex. And so the exponential growth rate of $a_\pm$ is given by

$$\sigma \equiv \omega_0 (m_0 A_\xi) \, \sigma_0 \quad \text{in which} \quad \sigma_0 \equiv |I_+ I_-^\star|^{1/2} \cos(\theta/2). \tag{13}$$

Here $A_\xi = a_0 k_0/\omega_0$ is the amplitude of the vertical displacement field, and θ is defined so that $\tan\theta$ is the ratio of the imaginary and real parts of $I_+ I_-^\star$. Of course if $f = 0$, then $I_\pm$ is pure real and $\theta = 0$. The prediction (13) is expected to be good provided the stream function amplitudes, $a_\pm$, of the sibling waves remains much smaller than the stream function amplitude, a_0, of the parent.

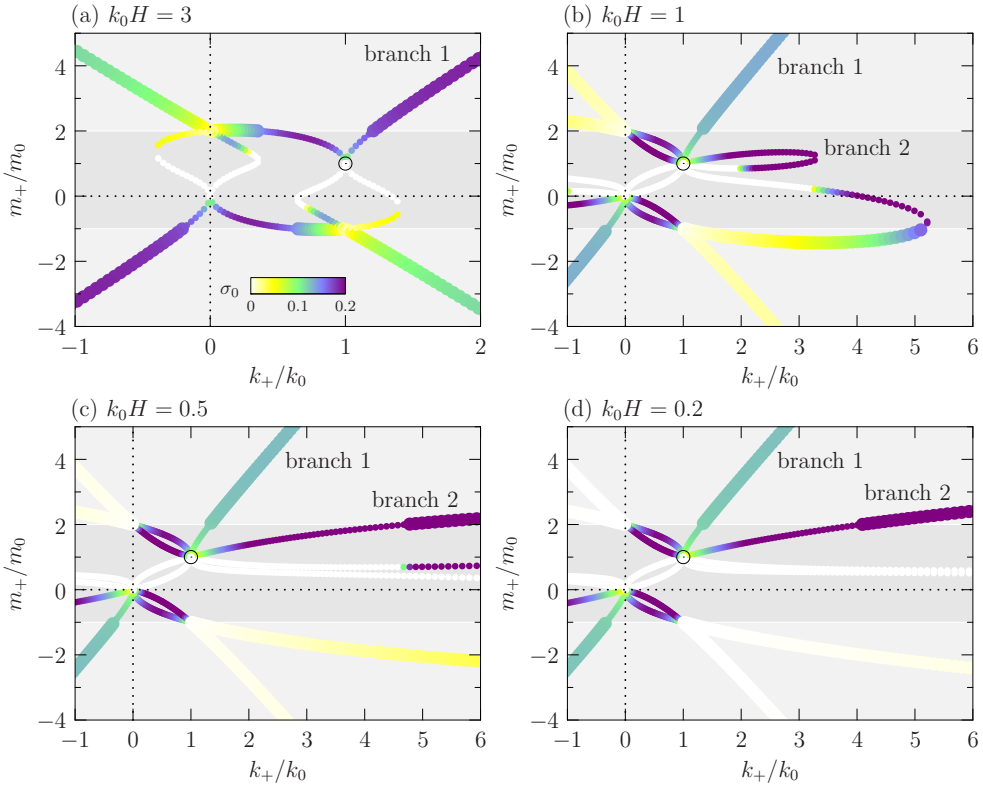

FIG. 1. Values of the sibling wave number (k_+, m_+) with component normalized respectively by the parent wave number (k_0, m_0) shown in four cases for a mode-1 wave, with $f = 0$ and values of k_0H as indicated. Pairs of sibling waves both with vertical wavelength smaller than H are allowed in the light gray-shaded regions. The nondimensional growth rate, σ_0 is indicated by color with scale indicated in (a). Sibling waves with the largest growth rate having $k_+ > k_0$ in the case $k_0H = 3$, and by extension to cases with $k_0H = 1$, 0.5, and 0.2 are denoted by "branch 1"; sibling waves with the highest growth rate appearing for $k_0H = 1$, 0.5, and 0.2 are denoted "branch 2."

As will be shown, σ_0 is of order 0.1. Also, in uniformly stratified fluid, the waves are overturning if $m_0A_\xi \geqslant 1$. Hence (13) shows that the growth rate relative to the parent mode frequency is on the order of a tenth the amplitude of the waves relative to the overturning amplitude. Of course, for low-mode internal tides, the amplitude is far below overturning. Hence the time for resonant growth of sibling waves from the parent is very much longer than the period of the parent mode. And because the internal tide frequency is on the order of f at midlatitudes, this suggests that TRI should take weeks to grow to non-negligible amplitudes.

E. Empirical results

As in Fig. 5 of Bourget *et al.* [22], Fig. 1 shows normalized values of the wave number (k_+, m_+) associated with one of the pair of sibling waves in the resonant triad with the parent having wave number (k_0, m_0). It is understood that the other sibling has wave number $(k_-, m_-) = (k_0, m_0) - (k_+, m_+)$. In each plot the middle region, for which $-1 < m_+/m_0 < 2$, is shaded medium gray as a reminder that sibling waves with $|m_+| < m_0$ or $|m_-| < m_0$ are not permitted when spawned by a mode-1 internal wave in uniform stratification because their half-wavelength is larger than the vertical extent of the domain. Likewise the points representing values of $m_+(k_+)$ are smaller within

this prohibited region. For each sibling wave number (k_+, m_+), the values of $I_\pm$ in Eq. (10) can be computed. Thus, for given vertical displacement amplitude A_ξ, the predicted growth rate of the siblings can be found using (13). In Fig. 1 the nondimensional growth rate, σ_0, is illustrated by the color of each point.

The curves in Fig. 1 a are similar to those appearing in Fig. 5 of Bourget *et al.* [22] who examined the case with $k_0 = m_0 (= \pi)$. The branch for $k_+ > k_0$ with the largest growth rate emanates upward to the right. A second set of unstable sibling waves also exists corresponding to the branch emanating downward to the right. However, its growth rate is significantly smaller.

For a parent mode that is more hydrostatic (having smaller k_0/m_0) the normalized growth rate corresponding to the up- and rightward branch decreases while a new branch develops with larger corresponding growth rate. This branch is evident in the case with $k_0 H = 1$ [Fig. 1(b)], but the corresponding vertical wave numbers of the sibling waves are too small to be manifest in the vertically bounded domain. For $k_0 H = 0.5$ and $k_0 H = 0.2$, this new branch is associated with sibling waves that both have sufficiently large vertical wave number. Separately, these curves have been computed taking into account the influence of Coriolis forces by setting $f = 0.01 N_0$. In all cases, the values of $m_+(k_+)$ are qualitatively similar even for the case with $k_0 H = 0.2$. However, some quantitative differences become apparent for small $k_0 H$, as examined next.

Corresponding to three of the four cases examined in Fig. 1, Fig. 2 focuses upon the properties of the sibling waves corresponding to the branches with the largest growth rates and $k_+ > k_0$. A fourth case considers the effect of nonzero f. In the case with $k_0 H = 1$, the vertical wave numbers, frequency and growth rate asymptote to constant values as k_+/k_0 becomes large. This lies in contrast to the study of Bourget *et al.* [22], who included viscous effects and so observed the decrease of the growth rate with increasing k_+/k_0. As might be expected from studies of parametric subharmonic instability, the frequency of both sibling waves is close to $\omega_0/2$ for large k_+/k_0. Correspondingly the relative vertical wave number of each sibling is close to twice the relative horizontal wave number, $m_\pm/m_0 \simeq 2k_\pm/k_0$, as follows directly from the dispersion relation for hydrostatic, nonrotating internal waves: $\omega \simeq Nk/m$.

In the case with $k_0 H = 0.5$ [Fig. 2(b)], a second branch corresponding to sibling waves with larger growth rate and frequencies much larger than the parent mode becomes manifest for $5 \lesssim k_+ \lesssim 11$, which is the range over which the sibling waves have $|m_\pm| > m_0$. The subharmonic branch has characteristics similar to those in the case with $k_0 H = 1$ such that the growth rate of the sibling waves is nearly constant for increasing k_+ and the frequencies are close to half that of the parent mode. Similar behavior occurs in the case with $k_0 H = 0.2$ and $f = 0$ [Fig. 2(c)] except that here the superharmonic branch exists with $|m_\pm| > m_0$ for much larger k_+, with the growth rate increasing as an approximate power law with k_+. The superharmonic behavior is similar with the inclusion of background rotation [Fig. 2(d)]. But in this case the subharmonic sibling waves exhibit a peak in their growth rate for k_+ comparable to k_0.

While these results suggest that superharmonic sibling waves should dominantly be excited through TRI from a hydrostatic parent mode, the simulations that follow will show that only subharmonic sibling waves develop. The near-uniformity of the growth rate for subharmonic sibling waves developing from a parent wave in inviscid nonrotating fluid suggests that one might expect to see the emergence of broad-banded wave beams oriented at an angle $\Theta \simeq \sin^{-1}[\omega_0/(2N_0)]$ to the horizontal and with slope $\simeq k_0/(2m_0) = H/\lambda_0$: half the effective slope of the parent wave. On the other hand, because the growth rate of subharmonic sibling waves in rotating fluid peaks at relatively small k_+/k_0, one might expect more narrow banded beams in this case. In fact, the numerical simulations presented below show that the subharmonic sibling waves are manifest as narrow-banded beams in all cases.

III. SIMULATIONS: SETUP AND ANALYSIS METHODS

The numerical model solves the fully nonlinear equations of motion for a horizontally periodic internal mode with free-slip upper and lower boundary conditions in arbitrary though stable

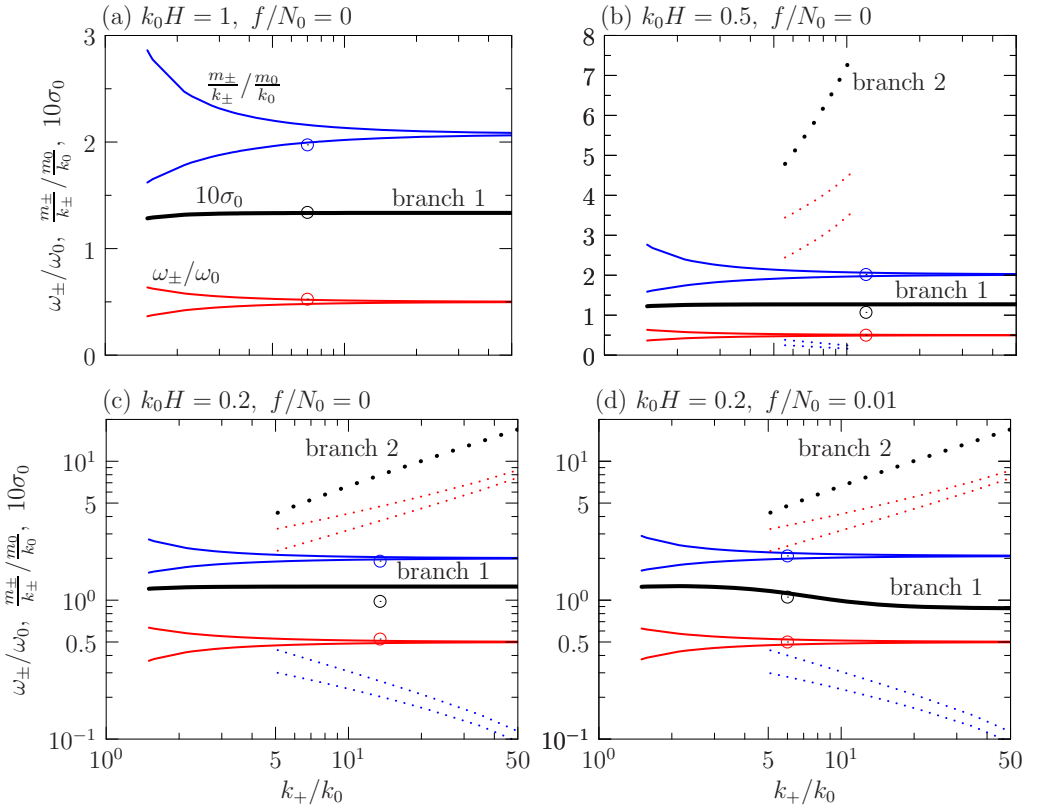

FIG. 2. Relative wave number ratio (blue), frequency (red), and the nondimensional growth rate σ_0 (thick black) computed for four different parent waves with k_0H and f/N_0 specified as indicated. Solid (dotted) lines give the predicted values corresponding to branch 1 (branch 2) as indicated in Fig. 1. Open circles correspond to the relative wave number ratio (blue), frequency (red), and nondimensional growth rate (black) measured in corresponding numerical simulations with $A_\xi = 0.01H$. Note that the ordinate in (a) and (b) is on a linear scale, whereas the ordinate in (c) and (d) is on a log scale. In all cases k_+/k_0 is plotted on a log scale, as indicated in the bottom plots.

stratification with and without uniform background rotation [18]. The code is effectively two-dimensional, meaning that the fields are spanwise uniform (in the y direction); the equations are solved in the x-z plane. Thus, with the inclusion of dissipative terms in the momentum and internal energy equation, (1) can be recast in terms of the spanwise vorticity (ζ) as well as the spanwise velocity (v) and buoyancy (b):

$$\zeta_t = -u\zeta_x - w\zeta_z + fv_z - b_x + \mathcal{D}_\zeta\zeta, \tag{14a}$$

$$b_t = -ub_x - wb_z - wN^2 + \mathcal{D}_b b, \tag{14b}$$

$$v_t = -uv_x - wv_z - fu + \mathcal{D}_v v, \tag{14b}$$

in which the subscripts on u, v, w, b, and ζ denote partial derivatives. In practice, the fields are represented by Fourier series components in the horizontal and in discrete evenly spaced steps in real space in the vertical. The operators for viscous and substance diffusion, $\mathcal{D}_\zeta$ and $\mathcal{D}_b$, are, respectively, defined to operate as Laplacian diffusion operators, $(1/\mathrm{Re})\nabla^2$ and $(1/\mathrm{PrRe})\nabla^2$, that act only upon disturbances with horizontal wave number greater than a cutoff k_c. In all cases $\mathrm{Re} \equiv N_0H^2/\nu = 100\,000$ and $\mathrm{Pr} = 1$. Although the Prandtl number is much smaller than that appropriate for relative

thermal/saline diffusion in water, it is sufficient to use this value since diffusion does not act upon the parent or sibling waves; it is included only for the purposes of numerical stability.

For given ζ at any time, the stream function is found by inverting the Poisson equation $\zeta = -\nabla^2\psi$ in mixed spectral-finite difference space. Given ψ, the u and w velocities are computed. Then (14) can be used to advance each of ζ, b, and v in time. Of course, if $f = 0$, it is unnecessary to evolve the spanwise velocity, v.

The simulations are initialized with a mode-1 internal wave in which the horizontally periodic domain contains two horizontal wavelengths of the mode. If $N = N_0$ is constant in a domain with $-H \leqslant z \leqslant 0$, the vertical structure of the mode is given in terms of the stream function by $\Psi(z) = \sin(m_0 z)$ [see (3)], in which $m_0 = \pi/H$. For simulations of waves in nonuniformly stratified fluid, the vertical structure, Ψ, is found using a Galerkin method, as described by Sutherland [18]. Thus the initial stream function corresponding to the parent wave is $\psi(x, z, t = 0) = a_0\Psi(z)\cos(k_0 x)$, in which a_0 and k_0 specified positive real values and $-2\pi/k_0 \leqslant x \leqslant 2\pi/k_0$. In practice, we specify A_ξ, the initial vertical displacement amplitude of the parent wave, and from this compute the stream function amplitude as $a_0 = (\omega_0/k_0)A_\xi$, in which ω_0 is given by the dispersion relation (5) if $N = N_0$, or is found empirically in the process of determining Ψ if N is nonconstant. Polarization relations are then used to initialize $\zeta(x, z, 0)$, $b(x, z, 0)$, and $v(x, z, 0)$.

As well as initializing the structure of the parent mode, small-amplitude spectral noise is superimposed. The noise mimics the midrange of the Garrett-Munk spectrum such that the stream function of the noise varies as $\omega^{-1/2}m^{-5/2}$, in which the frequency, ω, is determined from the dispersion relation for given wave number (k, m) of the noise. After specifying the spectrum, the noise field is inverse Fourier transformed to real space and the result multiplied by $N^2(z)$. The amplitude of the noise is set to be three orders of magnitude smaller than the amplitude of the parent wave. Simulations have also been performed with different noise spectra and amplitudes. In simulations where TRI was evident, the spectra and amplitudes were found moderately to influence the time for onset of TRI, but the growth rate and structure of sibling waves were found to be relatively insensitive to the prescribed noise.

The basic state fields are advanced in time using a leap-frog method for the advective and linear terms, with an Euler backstep taken every 20 time steps. In all simulations the time step was $0.005/N_0$. The diffusion operators are forward advanced to ensure numerical stability. The cutoff wave number used in the application of the selective diffusion operators $\mathcal{D}_\zeta$, $\mathcal{D}_b$, and $\mathcal{D}_v$ was set to be $k_c = 32k_0$.

In simulations with uniform stratification, the vertical was discretized by 129 evenly spaced points and the horizontal was decomposed spectrally by horizontal wave numbers between 0 and $128k_0$. Spatial and temporal resolution tests confirm that these choices provide satisfactory convergence with respect to the measured exponential growth rate of triadic resonance disturbances for sufficiently small-amplitude parent modes ($A_\xi \lesssim 0.02H$).

A standard diagnostic to assess the manifestation of TRI driven by the low-mode internal tides in the ocean involves the computation of bispectra, which reveals how pairs of waves interact to put energy into a third wave. With observational data being limited in spatial extent, it is typical to construct plots of bispectra from an ensemble of frequency spectra so as to examine favorable transfers from disturbances with frequencies ω_1 and ω_2 into a disturbance with frequency $\omega_0 = \omega_1 + \omega_2$ as measured at some fixed depth [11,12,25–27].

With numerical models the freedom exists to examine specifically how kinetic energy is put into or taken out of one wave by the quadratic interaction of two other waves [28,29]. Explicitly, neglecting fluxes $\mathbf{u}p$ associated with kinetic energy transport by waves, the change of kinetic energy per unit mass due to wave-wave interactions is given by

$$\frac{\partial}{\partial t}\left(\frac{1}{2}|\mathbf{u}|^2\right) = -\mathbf{u}\cdot(\mathbf{u}\cdot\vec{\nabla}\mathbf{u}), \tag{15}$$

in which $\mathbf{u}(x, z, t) = (u, v, w)$. In uniformly stratified fluid, the right-hand side of this expression may be rewritten in terms of the spatially Fourier transformed velocities $\hat{\vec{u}}(\mathbf{k}, t)$, in which

$\mathbf{k} = (k, m)$. In particular, focusing upon the interaction between the parent mode (having wave number $\mathbf{k}_0$) and a sibling wave (having wave number $\mathbf{k}_+$) so as to transfer energy to the other sibling (with wave number $\mathbf{k}_- = \mathbf{k}_0 - \mathbf{k}_+$), we have

$$\frac{\partial}{\partial t}\left(\frac{1}{2}|\mathbf{u}_-|^2\right) = \sum_{\mathbf{k}_+} \mathrm{Re}\{-(\hat{\mathbf{u}}_0 \cdot \imath\mathbf{k}_+)(\hat{\mathbf{u}}_+ \cdot \hat{\mathbf{u}}_-^\star) - (\hat{\mathbf{u}}_+ \cdot \imath\mathbf{k}_0)(\hat{\mathbf{u}}_0 \cdot \hat{\mathbf{u}}_-^\star)\}, \tag{16}$$

in which $\hat{\mathbf{u}}_0 = \hat{\mathbf{u}}(\mathbf{k}_0, t)$, $\hat{\mathbf{u}}_\pm = \hat{\mathbf{u}}(\mathbf{k}_\pm, t)$, Re{} denotes the real part of the enclosed expression, and the star denotes the complex conjugate. The terms in the sum represent the bispectrum which, for a given parent mode, is a function of the wave number vector (k_+, m_+).

In the consideration of TRI of an internal mode in nonuniformly stratified fluid, this approach is invalid because the parent mode is not sinusoidal in the vertical. Although one could expand the vertical structure as a Fourier series, this would falsely introduce a corresponding range of frequencies associated with each vertical Fourier mode. Recognizing that the parent mode is monochromatic in frequency and horizontal wave number, we take a new approach that acts as a hybrid between (16) and the observational oceanography approach of constructing bispectra from frequency spectra measured at a point in space. Because the growth of sibling waves occurs on a slow timescale compared with the frequency of the parent and sibling waves, we can construct a frequency spectrum from a time series that is long compared to the parent wave period but short compared to the e-folding time of the resonantly growing sibling waves. More precisely, we construct a horizontal time series of the stream function, $\psi(x, t; z_0)$, and horizontal velocity, $u(x, t; z_0)$, at some depth z_0 and then double Fourier transform to construct the spectra $\hat{\psi}(k, \omega)$ and $\hat{u}(k, \omega)$. To compute the corresponding energy transfers in (k, ω)-space, we write the right-hand side of (15) explicitly in terms of a double sum over pairs of horizontal wave numbers and frequencies of expressions involving $\hat{\psi}$ and $\hat{u}$ alone. In doing so, we recognize that $\hat{v} = -\imath(f/\omega)\hat{u}$ and $\hat{w} = \imath k\hat{\psi}$. Also, because the vertical structure of the stream function, $\Psi(z)$, satisfies (3), the terms involving $\partial_z u = -\partial_{zz}\psi$ in Eq. (15) can be recast in Fourier space in terms of $\hat{\psi}$ with N^2 being evaluated at $z = z_0$. The corresponding bispectrum is

$$\begin{aligned} B(k_+, \omega_+) = \mathrm{Re}\big\{&-\imath\hat{u}_-^\star[(\beta_+ k_+ + \beta_0 k_0)\hat{u}_0\hat{u}_+ + k_0 k_+(\beta_+\alpha_+ k_+ + \beta_0\alpha_0 k_0)\hat{\psi}_0\hat{\psi}_+] \\ &-\imath\left(k_+^2 - k_0^2\right)\hat{\psi}_-^\star[k_+\hat{u}_0\hat{\psi}_+ - k_0\hat{u}_+\hat{\psi}_0]\big\}. \end{aligned} \tag{17}$$

Here we have defined $\alpha_i \equiv (N^2(z_0) - \omega_i^2)/(\omega_i^2 - f^2)$ and $\beta_i \equiv 1 - f^2/(\omega_-\omega_i)$ where the subscript i represents 0 or +. The subscripts 0, +, and − on $\hat{\psi}$ and $\hat{u}$ respectively indicate whether the argument of the spectral field is (k_0, ω_0), (k_+, ω_+) or $(k_-, \omega_-) = (k_0, \omega_0) - (k_+, \omega_+)$.

IV. SIMULATIONS RESULTS

Here we present the results of numerical simulations showing TRI developing from horizontally periodic mode-1 internal waves in uniform stratification. The simulations examined the occurrence of TRI of a horizontally periodic, vertical mode-1 parent wave as it depended upon its amplitude and horizontal wave number as well as the influence of background rotation. Generally it was found that significant time passed before coherent resonant sibling waves emerged and grew exponentially.

The results from a simulation with $k_0 H = 1$ and $A_\xi = 0.02H$ are shown in Figs. 3–5. Figure 3 shows snapshots of the total and mode-filtered horizontal velocity field at three times. The latter is found by Fourier-filtering disturbances with horizontal wave number $k = k_0$. At time $t = 3000/N_0$, the total horizontal velocity field appears the same as it does initially, although the filtered horizontal velocity at this time reveals a weak disturbance dominated by structures with horizontal wave number $2k_0$. The clear appearance in the filtered horizontal velocity of coherent internal wave beams is evident at time $t = 5000/N_0$, their amplitude being large enough to distort significantly the total horizontal velocity field. As these sibling waves continue to grow in amplitude, other high wave number disturbances grow, resulting in a less coherent perturbation.

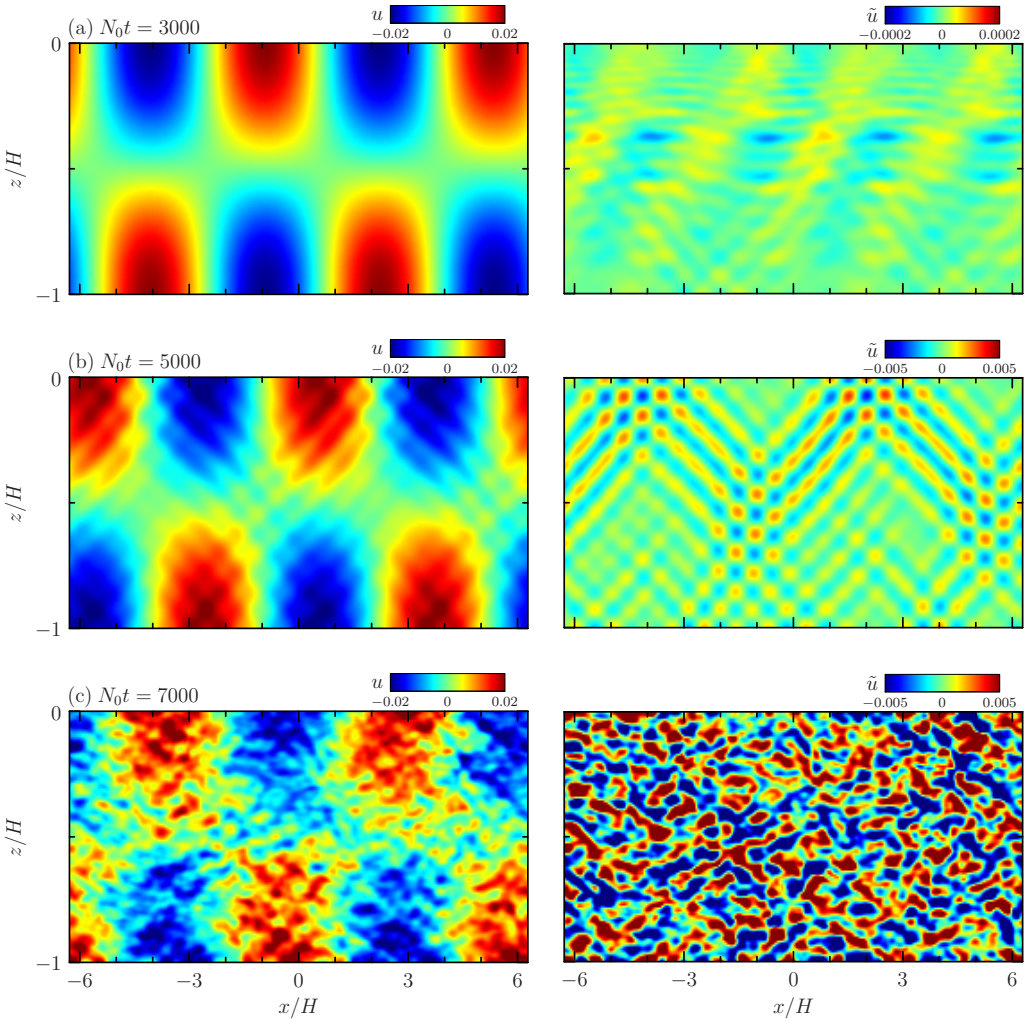

FIG. 3. Total horizontal velocity (left) and mode-filtered horizontal velocity (right) from a simulation with two horizontal wavelengths of a mode-1 internal mode with $k_0H = 1$ and $A_\xi = 0.02H$ shown at nondimensional times (a) $N_0t = 3000$, (b) 5000, and (c) 7000. The values of velocity are represented by colors as indicated to the upper right in each plot. In all cases, the fields are shown in a frame of reference moving with the phase speed of the wave so that the phase is fixed.

It is clear that the sibling waves in Fig. 3(b) (right) are not uniform over the domain but are manifest as localized beams coinciding with nodes of the horizontal velocity field at the top and bottom of the domain. The origin of the beam development is revealed in Fig. 4, which shows vertical and horizontal time series of the mode-filtered horizontal velocity field between nondimensional times $N_0t = 4000$ and 5000. These time series are extracted from mode-filtered snapshots in a frame of reference moving with the horizontal phase speed of the parent wave. In order to focus on the structure of the exponentially growing waves, the color field shows values of

$$\{\tilde{u}\} \equiv \mathrm{sgn}(\tilde{u}) \ln(|\tilde{u}|). \tag{18}$$

From the vertical time series of $\{\tilde{u}\}(x = 0, z, t)$ it is clear that the waves first develop in the middle of the domain and then extend over time to the upper and lower boundaries as the beam grows in

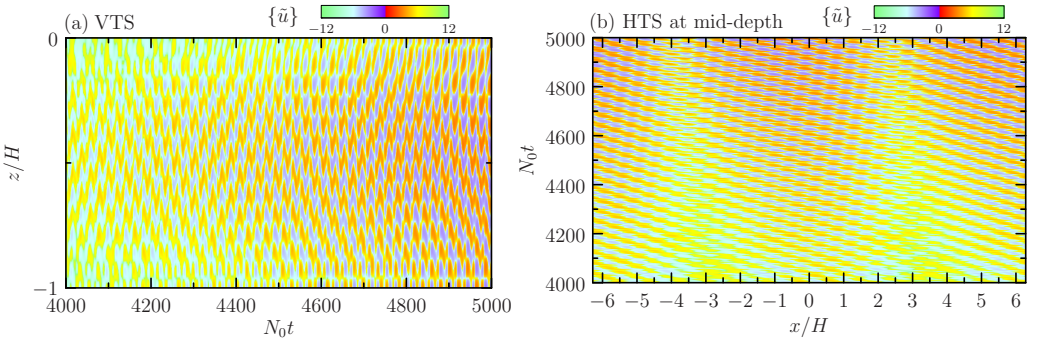

FIG. 4. (a) Vertical time series at $x = 0$ and (b) horizontal time series at half-depth of $\{\tilde{u}\} \equiv \mathrm{sgn}(\tilde{u}) \ln(|\tilde{u}|)$ shown over nondimensional times $4000 \leqslant N_0 t \leqslant 5000$. In both cases the mode-filtered horizontal velocity $\tilde{u}$, is fixed in a frame of reference moving with the phase speed of the wave.

amplitude. The spatial development is reminiscent of the laboratory experiments of Benielli and Sommeria [14,15] and Joubaud *et al.* [16] in which subharmonic instabilities developing from a parent mode were found to grow first near the middle of their tanks. In the simulations presented here, the domain is horizontally periodic. Nonetheless, the horizontal time series constructed from the filtered horizontal velocity at middepth in the domain, $\{\tilde{u}\}(x, z = H/2, t)$, shows the waves first develop about the region where the horizontal velocity is rightward above and leftward below. The dominant vertical wave number, $m_\star$, of the growing resonant disturbances is measured by determining the peak of the spectrum found from the Fourier cosine transform of $\tilde{u}(x = 0, z, t)$ at $N_0 t = 5000$. Likewise the dominant horizontal wave number, $k_\star$, is found from the Fourier transform of $\tilde{u}(x, z = H/2, t)$ at $N_0 t = 5000$. Explicitly, in terms of the respective wave numbers of the parent mode, we find $m_\star = 12.9 m_0$ and $k_\star = 7.00 k_0$. Their ratio, 1.84, is indicated by the blue circle to the right of Fig. 2(a). Consistent with theory, the ratio is close to 2.

A plot of the total disturbance energy, KE, in Fig. 5 shows that it fluctuates about values close to $e^{-12} \simeq 6 \times 10^{-6}$ of the kinetic energy, KE_0, of the parent mode until shortly before nondimensional time $N_0 t = 4000$ when the disturbance energy rises exponentially. After

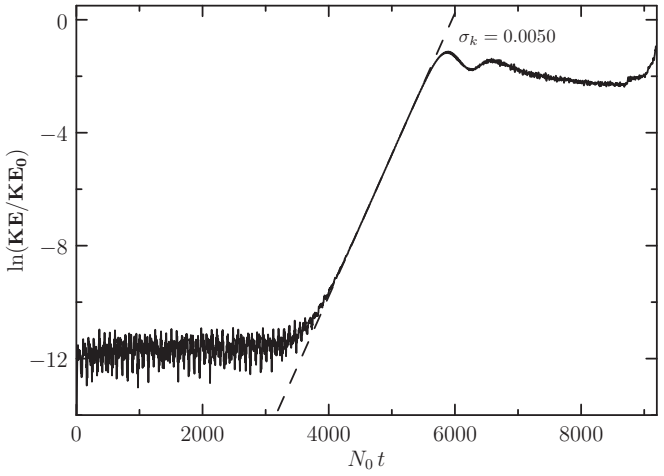

FIG. 5. Log plot of the normalized disturbance kinetic energy plotted versus time. The best-fit line to the kinetic energy curve with slope σ_k (dashed black line) is determined over times $4500 \leqslant N_0 t \leqslant 5500$.

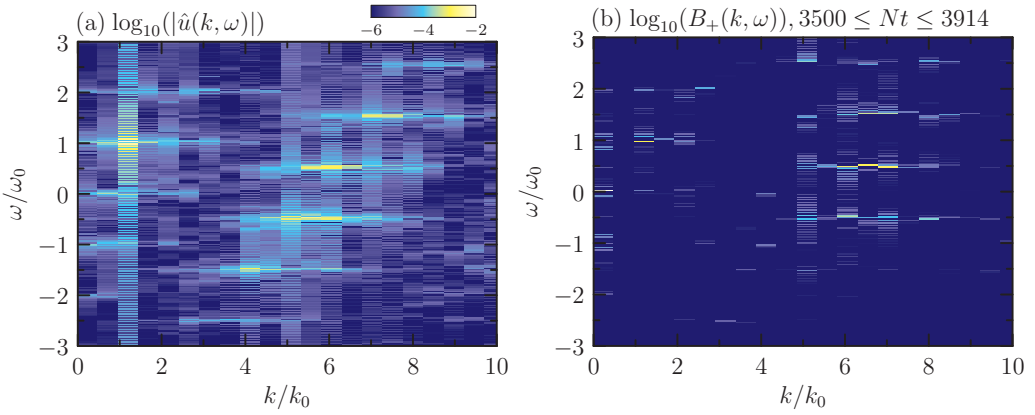

FIG. 6. (a) Log of the magnitude of the spectrum of horizontal velocity determined from horizontal time series at $z_0 = -0.25H$ spanning 20 periods of the parent mode starting at $Nt = 3500$, when the development of superharmonics becomes evident. (b) Log of the corresponding bispectrum for values of $B > 0$. In both plots, negative frequencies correspond to leftward-propagating waves.

$N_0 t \simeq 5500$, the disturbance energy saturates. Clearly the time over which exponential growth occurs is associated with the formation of the coherent beams evident in Fig. 3(b) (right). The kinetic energy growth rate, σ_k, is found from the slope of the best-fit line through the plot of $\log(\mathrm{KE}/\mathrm{KE}_0)$ over times when this value lies between -8 and -4. For the example shown in Fig. 5, the relative kinetic energy growth rate is $\sigma_k/N_0 \simeq 0.005014\ (\pm 1.3 \times 10^{-6})$.

For comparison with theory, the kinetic energy growth rate is recast in terms of the growth rate of the amplitude of the resonant disturbances as given by (13). The result is then normalized for comparison with the predicted nondimensional growth rate, σ_0, in Eq. (13). Explicitly, we compute the numerically determined nondimensional growth rate as

$$\sigma_0^\star = \frac{\sigma_k}{2\omega_0 m_0 A_\xi}. \tag{19}$$

For the case shown in Fig. 5, we find $\sigma_0^\star \simeq 0.134$, which is in very good agreement with the predicted value of σ_0, as indicated in Fig. 2(a).

As another diagnostic check, we compute the spectrum of the horizontal velocity $\hat{u}(k, \omega)$, from the horizontal time series constructed at $z = -0.375H$ for times between $N_0 t = 3500$ and 3914, a duration of 20 periods of the parent wave. As shown in Fig. 6(a), there is a clear peak at the frequency and horizontal wave number of the parent mode as well as a sequence of peaks at $(k/k_0, \omega/\omega_0) = (4, -1.5), (6, -0.5), (7, 0.5), (7, 1.5)$. The bispectrum computed from this spectrum [Fig. 6(b)] is strongly peaked at $k = 7(\pm 0.5)k_0$ and $\omega = 0.5(\pm 0.25)\omega_0$, consistent with the spectral analysis discussed above. While the subharmonic frequency is consistent with theory, it is unclear why the growth of the sibling waves (at $k_+ = 7k_0$ and $k_- = 6k_0$) is so narrow banded given that the growth rate of subharmonic sibling waves is predicted to be nearly constant for large k_+.

The detailed analysis above for the case of a parent mode with $k_0 H = 1, A_\xi = 0.02H$, and $f = 0$ clearly shows the emergence of quasimonochromatic internal wave beams through TRI, having frequency and growth rate consistent with theoretical predictions. The ratio of the relative vertical to horizontal wave number, being close to 2, is also consistent with theory.

In numerous simulations in which the parent mode wave number varied between $k_0 H = 0.1$ and 3 and its amplitude varied between $A_\xi = 0.01$ and 0.04, only subharmonic sibling waves were observed to grow, with their structure and growth rate being well represented by theory. For example, in Fig. 2 some of the simulation results are indicated by the open circles for comparison with theory. Overall, the results suggest that the theory for TRI of plane waves can reasonably be adapted to the

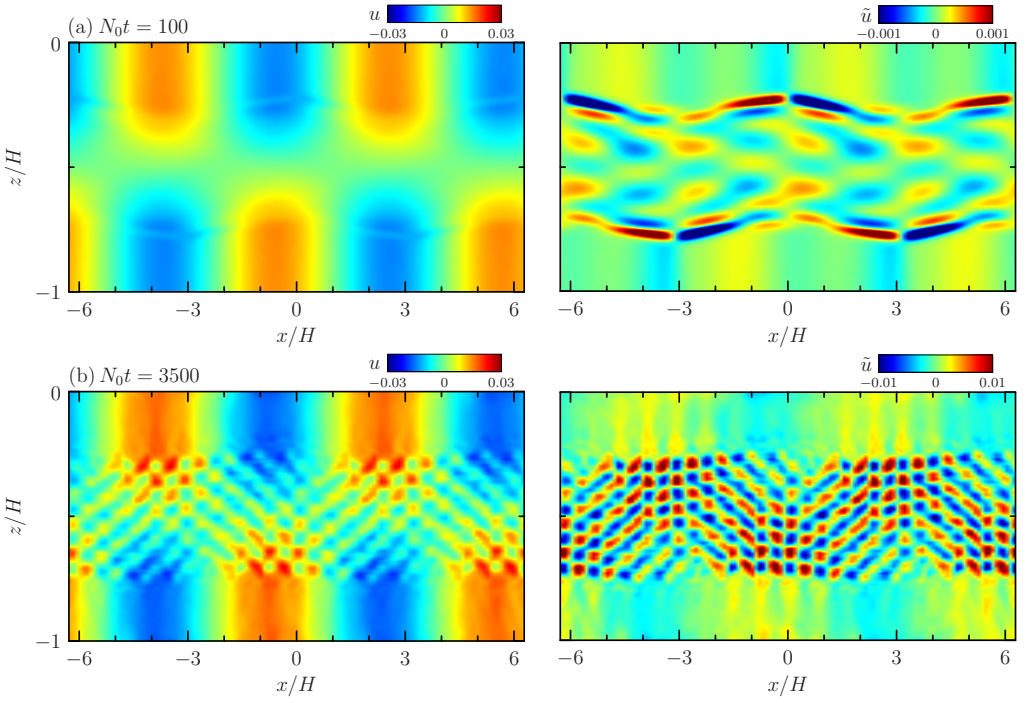

FIG. 7. Snapshots of the total (left) and mode-filtered (right) horizontal velocity shown at times (a) $N_0t = 100$ and (b) $N_0t = 3500$ from a simulation initialized with a mode having $k_0H = 1$ and $A_\xi = 0.02H$ in symmetric top-hat stratification with $N^2 \simeq N_0^2$ in the middle half of the domain and $N^2 = 0$ otherwise.

study of internal modes with the proviso that the confined vertical geometry results in the growth of subharmonics alone with the faster growing superharmonics being excluded. Reasons for this exclusion are discussed in Sec. VI.

V. NONUNIFORM STRATIFICATION

Simulations were also performed examining the evolution of internal modes in nonuniform stratification. Generally such modes self-interact so as directly to force superharmonic disturbances with twice the horizontal wave number and frequency (but, hence, the same phase speed) of the parent mode [17,18]. The forcing itself depends upon the gradient of the background squared buoyancy frequency, and so does not exist in uniformly stratified fluid. Although superharmonic disturbances immediately become evident, the question is whether sibling waves generated through TRI can eventually emerge.

As a simple extension of the above study of TRI occurring for modes in uniform stratification, we have performed simulations in which the stratification had an approximate symmetric top-hat structure ($N = N_0$ for $-3H/4 \lesssim z \lesssim -H/4$ and zero otherwise) in which the transition from the unstratified to stratified layer was modelled by hyperbolic tangent functions that transition over a distance $0.02H$, as described in van den Bremer *et al.* [24]. To capture the transition, the simulations were performed with a resolution consisting of 1025 evenly spaced points in the vertical.

Figure 7 shows that the occurrence of TRI in top-hat stratification is indeed possible. In this case, the parent mode had horizontal wave number $k_0\,H = 1$ and amplitude $A_\xi = 0.02H$. Its corresponding frequency was $\omega_0 = 0.277$. At early times [Fig. 7(a)] the forcing, being largest where N^2 transitions from the stratified to unstratified regions, results in superharmonic disturbances situated around $z = -0.25H$ and $-0.75H$. Because the superharmonic forcing frequency, $2\omega_0$, is

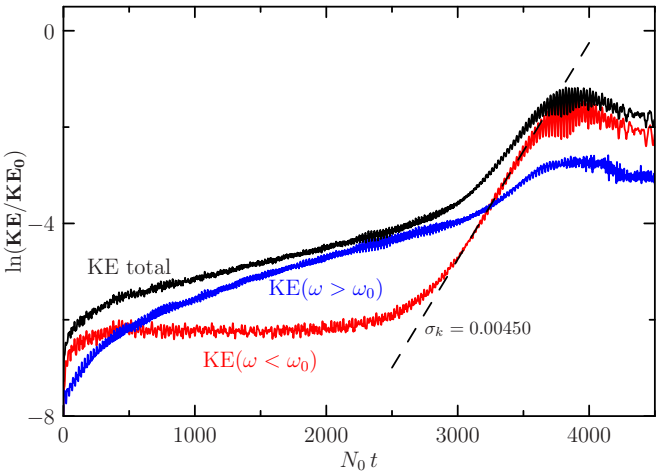

FIG. 8. Mode-filtered energy versus time for the simulation shown in Fig. 7, with the total energy (black) being the sum of energy associated with disturbances having frequency less than ω_0 (red) and greater than ω_0 (blue). The best-fit line through the red curve for $3000 \leqslant N_0 t \leqslant 3500$ shows exponential growth of subharmonics with rate σ_k indicated.

less than N_0, the disturbances at the flanks of the stratified region can excite superharmonic waves that propagate vertically into the stratified region. But such disturbances are not a manifestation of TRI.

The development of TRI is apparent at time $N_0 t = 3500$, as shown in Fig. 7(b). As in the simulation of a parent mode in uniform stratification, wave beams emerge with $(k_\star/k_0, m_\star/m_0) \simeq (9, 17)$. The internal wave beams constructively reflect from the bottom and top extent of the stratified region. The disturbance kinetic energy is shown in Fig. 8. After Fourier transforming the velocity field over the time of the simulation, the disturbance kinetic energy is subdivided into the fraction associated with disturbances having frequency larger than that of the parent mode (blue curve) and that having frequency subharmonic to the parent mode (red curve). Although initially most of the disturbance energy is associated with superharmonics, the rapid exponential growth of subharmonics becomes apparent after time $N_0 t \simeq 3000$. The growth rate associated with this energy is $\sigma_k = 0.00450\ (\pm 0.00002) N_0$, about 10% lower than the growth rate measured for subharmonic disturbances arising in corresponding simulations with uniformly stratified fluid.

The spectrum of $\hat{u}(k, \omega)$ was computed for 20 parent-mode periods after $N_0 t = 3200$, as shown in Fig. 9(a). This reveals staggered peaks at half-integer frequencies dominantly for k/k_0 in a range between 6 and 9. However, the corresponding bispectrum in Fig. 9(b) shows multiple peaks, with the largest occurring for frequency $\omega^\star \simeq 1.5\omega_0$. Clearly the complicated wave field from which TRI appears to develop makes a bispectral analysis less conclusive about the origin of the waves as having originated from a simple triad between two subharmonic sibling waves and the parent mode. However, the structure of the wave beams that emerge after $N_0 t = 3200$ and their growth rate (which depends on the amplitude of the wave that generates them) suggests they do indeed arise primarily through resonant interaction with the parent mode and not through interaction with the superharmonics.

TRI eventually emerged because the depth of the stratified region was set to allow the beams to interact constructively upon reflection from the flanks of the stratified layer. In other simulations (not shown) in which the stratified layer was more or less than half-depth, no clear emergence of triadic resonance instability was apparent through the myriad disturbances arising from the persistent superharmonic forcing. This suggests that the eventual emergence of beams produced by TRI shown in Fig. 7, relied on the depth of the stratified region being half the total ambient fluid

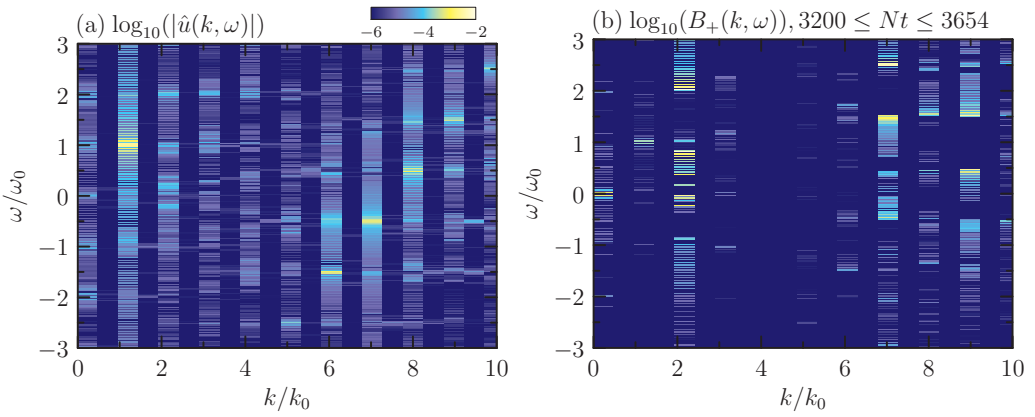

FIG. 9. As in Fig. 6, but for the simulation with top-hat stratification shown in Fig. 7, showing (a) the spectrum of horizontal velocity and (b) the corresponding bispectrum computed for 20 periods of the parent mode starting at $Nt = 3200$. The spectrum, $\hat{u}$, is determined from a horizontal time series at $z_0 = -0.325H$.

depth so the beams interfere constructively as they successively reflect from the top and bottom of the stratification.

Also crucial for the emergence of TRI in the top-hat simulation shown in Fig. 7 was the symmetry of the stratification. If the extent of the stratified region was shifted from being centered around middepth, then TRI was not observed even after very long times. Instead the mode-filtered energy was dominated by low-mode superharmonics whose energy oscillates in time, as shown in Fig. 10(a).

There was also no evidence for TRI in simulations with stratification more representative of the ocean according to $N^2 = N_0^2 \exp(z/D)$ or, for the purposes of comparison with Hazewinkel and Winters [10], $N(z) = N_0/(1 - z/z_0)$ for $-H \leqslant z \leqslant 0$. These simulations were chosen to have parameters representative of internal tides in the ocean. Corresponding to internal tides in a $H = 4$ km deep ocean with a horizontal wavelength of 100 km and a maximum surface horizontal velocity of 10 cm/s, we set $A_\xi = 0.002H$ and $k_0 H = 0.2$. In the simulation with exponential stratification the thermocline was taken to have depth $D = 0.2H$. The stratification and Coriolis frequency were respectively taken to have characteristic values of $N_0 = 10^{-2}\,\mathrm{s}^{-1}$ and $f = 0.01N_0$. Through the numerical solution of (3), the frequency of the mode-1 parent wave was found to be $0.027N_0$. By extension of the theory for internal modes in uniform stratification through (13), the growth rate of subharmonics is anticipated to be on the order $\sigma \simeq 0.1\omega_0(\pi/D)A_\xi \sim 10^{-4}N_0$. Here we have supposed the vertical wave number, m_0, scales with the thermocline depth, D, and we have taken $\sigma_0 \sim 0.1$. With $N_0 = 10^{-2}\,\mathrm{s}^{-1}$, the predicted growth rate corresponds to an e-folding time scale of 12 days. This prediction is consistent with the simulations of Hazewinkel and Winters [10] (see their Fig. 2), who observed the growth of subharmonics by nine orders of magnitude over 250 days. Nonetheless, in our simulations with a vertical resolution of 1025 points and with a Garrett-Munk spectrum of noise, we did not observe any growth of subharmonics even after running for times up to $10^5 N_0$. Neither was evidence for TRI apparent in simulations run with different spectra and amplitudes of noise. Instead, like the simulations with a shifted top-hat stratification [Fig. 10(a)], superharmonics were found to grow and decay periodically in time, as shown in Fig. 10(b). It is now understood that this oscillatory behavior results from near-resonant beating between the parent mode and superharmonic which itself is close to a pure mode-1 disturbance [23].

While the spectrum and amplitude of the background noise in the simulations of Hazewinkel and Winters [10] may have played some role in the emergence of subharmonics, it seems likely that the important difference between their simulations and ours is that they forced the waves from a left boundary and damped the waves as they approached the right boundary of their domain. Thus

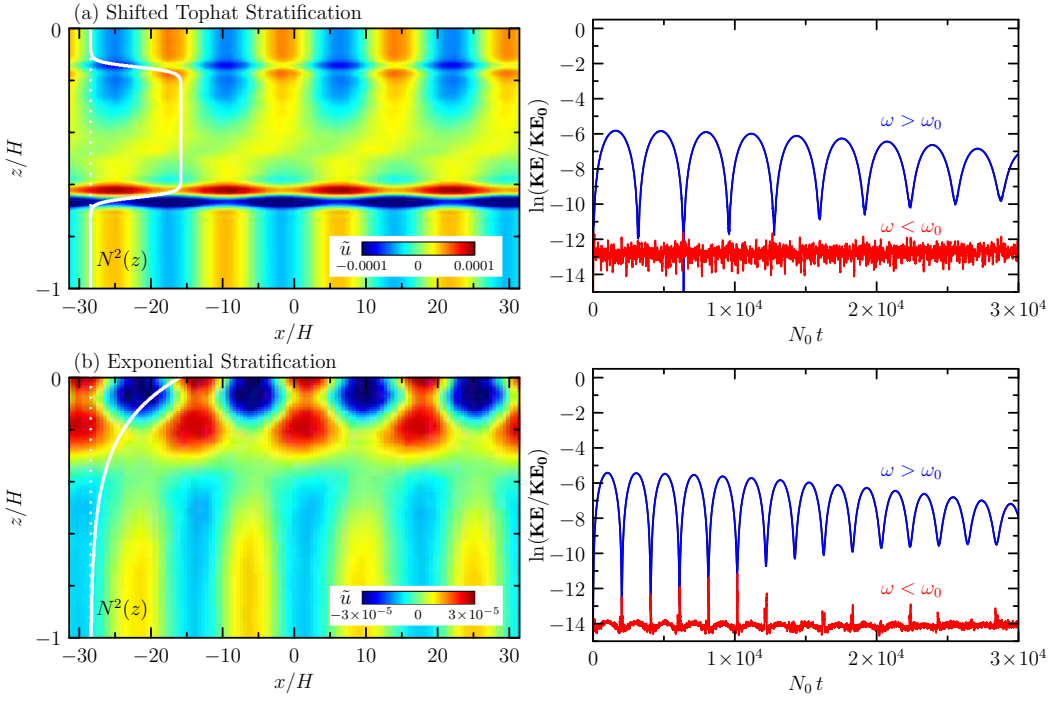

FIG. 10. Results from simulations with (a) shifted top-hat stratification and (b) exponential stratification showing, as in right plots of Fig. 7, mode-filtered snapshots at $N_0 t = 30\,000$ (left) and, as in Fig. 8, the evolution of the mode-filtered energy partitioned into low and high frequency disturbances (right) The structure of the stratification is superimposed in white on left plots. In both simulations $A_0 = 0.002H$, $k = 0.2H$.

their simulations did not show any significant development of superharmonics, as these propagate in the direction of the parent mode and would have been damped at the right boundary. By contrast, the subharmonics have both rightward and leftward group velocity and so could develop to finite amplitude within their computational domain.

VI. DISCUSSION AND CONCLUSIONS

We have constructed predictions for the structure and growth rate of pairs of sibling waves that develop from monochromatic internal plane waves in uniform stratification. While mathematically straightforward to apply these results to a horizontally periodic mode-1 internal wave, the vertical confinement of the mode introduces extra restrictions on what sibling waves might develop through triadic resonant instability. Clearly the vertical wave number of both sibling waves must be greater than that of the parent mode so that at least a half vertical wavelength can fit in the domain. So that the waves interfere constructively upon reflection from the upper and lower boundaries, the vertical wave number of the sibling waves in fact should be at least twice that of the parent mode.

The constructive interference of sibling waves reflecting from the upper and lower boundaries apparently places an additional restriction on what waves grow through TRI. Although, for a horizontally long mode, the fastest growth is predicted for sibling waves that have frequency much larger than the parent, simulations show that the dominant sibling waves that emerge have close to half the frequency of the parent and grow at the second fastest rate predicted by theory. These sibling waves are manifest as beams that reflect from the upper and lower boundaries. That the ratio of their vertical to horizontal wave number, $m_\pm/k_\pm$, is close to twice the corresponding ratio for the parent mode means that for a beam that originates at middepth and then reflects from the top or bottom

boundary, it returns at middepth at the same point in phase of the parent mode. Having observed in simulations that the amplitude of the sibling waves is first largest at middepth, reaffirms the importance of the vertically confined geometry in selecting the subharmonic over the theoretically faster growing superharmonic sibling waves. Including background rotation, the sibling waves that emerge have smaller horizontal and vertical wave number.

The predictions serve in part to validate numerical simulations of the evolution of a mode-1 internal mode in which sibling waves are indeed observed eventually to grow exponentially at the growth rate and with the frequency and structure predicted for the subharmonic branch of TRI. This resonant interaction is also confirmed by a newly formulated bispectral analysis of horizontal time series of the flow. However, we find that the case of uniform stratification is special. Only in simulations with symmetric top-hat stratification in which the depth of the stratified region was half the total depth did we observe the eventual growth of subharmonics through TRI. Like simulations with uniform stratification, the geometry of this stratification permitted constructive interference between successive upward and downward propagating beams of sibling waves that travel horizontally by one parent-mode wavelength after two reflections. In all other cases examined, the generation of superharmonics through the self-interaction of the parent mode in nonuniform stratification dominated the evolution of the system over times much longer than the predicted e-folding time for growth of sibling waves.

On the one hand, these results suggest that TRI of the low-mode internal tides in the ocean may not be a significant pathway for energy to transfer from large to small scale. However, some qualification is required in light of the results of Hazewinkel and Winters [10], who did observe the emergence of subharmonic beams in their simulations of two parent modes coevolving in nonuniformly stratified fluid representative of the ocean. Furthermore, observations of the internal tide north of Hawaii near 29°N were suggestive of the occurrence of subharmonic instability putting (albeit modest) energy into near-inertial motions. This suggests that if TRI is important for the partial breakdown of oceanic internal tides, then other factors such as background noise and the modulation of the tides likely play a role in the emergence of sibling waves.

ACKNOWLEDGMENT

This research was performed through funding from the Natural Sciences and Engineering Research Council (NSERC) of Canada.

APPENDIX: SOLUTION METHOD FOR RESONANT TRIADS IN UNIFORM STRATIFICATION

Consider a parent wave with known vertical wave number m_0 ($= \pi/H$) for a mode-1 wave), horizontal wave number k_0, and corresponding frequency ω_0, given by (5). The frequency of the two sibling waves are related to the parent wave by (8c). Rewriting this expression as $(\omega_0 \pm \omega_+)^2 = \omega_-^2$, using the dispersion relations (5) and (7), and isolating the resulting term involving a square root on the left-hand side gives

$$2\omega_0\sqrt{\frac{N_0^2k_+^2 + f^2m_+^2}{k_+^2 + m_+^2}} = \omega_0^2 + \frac{N_0^2k_+^2 + f^2m_+^2}{k_+^2 + m_+^2} - \frac{N_0^2k_-^2 + f^2m_-^2}{k_-^2 + m_-^2}.$$

Squaring both sides, multiplying through by $(k_+^2 + m_+^2)^2(k_-^2 + m_-^2)^2$, and using (8a) and (8b) to replace (k_-, m_-) with $(k_0 \pm k_+, m_0 \pm m_+)$, gives a degree-8 polynomial for m_+ as it depends upon k_+, with the coefficients otherwise depending upon the known values of N_0, f, m_0, k_0, and ω_0.

In practice, for specified k_+ the real roots of the polynomial are found using Matlab's "solve" function. For each resulting value of m_+, the values of (k_-, m_-) are found using (8a) and (8b), and $\omega_\pm$ is found using (7). The result is checked by confirming that the frequency resonance condition (8c) holds. This procedure is then repeated for different values of k_+. In practice, by symmetry it

is sufficient to examine a range of k_+ from $k_0/2$ and above. Values of m_+ for $k_+ < k_0/2$ are found from the values of m_- for $k_+ > k_0/2$ using $m_+(k_0 - k_+) = m_0 - m_-(k_+)$.

[1] R. Ferrari and C. Wunsch, Ocean circulation kinetic energy: Reservoirs, sources, and sinks, Ann. Rev. Fluid Mech. **41**, 253 (2009).

[2] J. M. Klymak, J. N. Moum, J. D. Nash, E. Kunze, J. B. Girton, G. S. Carter, C. M. Lee, T. B. Sanford, and M. C. Gregg, An estimate of tidal energy lost to turbulence at the Hawaiian Ridge, J. Phys. Oceanogr. **36**, 1148 (2006).

[3] Z. Zhao, M. H. Alford, J. B. Girton, L. Rainville, and H. Simmons, Global observations of the open-ocean mode-1 M_2 internal tides, J. Phys. Oceanogr. **46**, 1657 (2016).

[4] J. A. MacKinnon, Z. Zhao, C. B. Whalen, A. F. Waterhouse, D. S. Trossman, O. M. Sun, L. C. St. Laurent, H. L. Simmons, K. Polzin, R. Pinkel, A. Pickering, N. J. Norton, J. D. Nash, R. Musgrave, L. M. Merchant, A. V. Melet, B. Mater, S. Legg, W. G. Large, E. Kunze, J. M. Klymak, M. Jochum, S. R. Jayne, R. W. Hallberg, S. M. Griffies, S. Diggs, G. Danabasoglu, E. P. Chassignet, M. C. Buijsman, F. O. Bryan, B. P. Briegleb, A. Barna, B. K. Arbic, J. K. Ansong, and M. H. Alford, Climate process team on internal wave-driven ocean mixing, Bull. Am. Meteorol. Soc. **98**, 2429 (2017).

[5] T. Dauxois, S. Joubaud, P. Odier, and A. Venaille, Instabilities of internal gravity wave beams, Annu. Rev. Fluid Mech. **50**, 131 (2018).

[6] C. Staquet and J. Sommeria, Internal gravity waves: From instabilities to turbulence, Ann. Rev. Fluid Mech. **34**, 559 (2002).

[7] T. Hibiya and M. Nagasawa, Latitudinal dependence of diapycnal diffusivity in the thermocline estimate using a finescale parameterization, Geophys. Res. Lett. **31**, L01301 (2004).

[8] T. Hibiya, M. Nagasawa, and Y. Niwa, Global mapping of diapycnal diffusivity in the deep ocean based on the results of expendable current profiler (XCP) surveys, Geophys. Res. Lett. **33**, L03611 (2006).

[9] J. A. MacKinnon and K. B. Winters, Subtropical catastrophe: Significant loss of low-mode tidal energy at 28.9°, Geophys. Res. Lett. **32**, L15605:1 (2005).

[10] J. Hazewinkel and K. B. Winters, PSI of the internal tide on a β plane: Flux divergence and near-inertial wave propagation, J. Phys. Oceanogr. **41**, 1673 (2011).

[11] J. A. MacKinnon, M. H. Alford, O. Sun, R. Pinkel, Z. Zhao, and J. Klymak, Parametric subharmonic instability of the internal tide at 29°N, J. Phys. Oceanogr. **43**, 17 (2013).

[12] J. K. Ansong, B. K. Arbic, H. L. Simmons, M. H. Alford, M. C. Buijsman, P. G. Timko, J. G. Richman, J. F. Shriver, and A. J. Wallcraft, Geographical distribution of diurnal and semidiurnal parametric subharmonic instability in a global ocean circulation model, J. Phys. Oceanogr. **48**, 1409 (2018).

[13] D. Olbers, F. Pollmann, and C. Eden, On PSI interactions in internal gravity wave fields and the decay of baroclinic tides, J. Phys. Oceanogr. **50**, 751 (2020).

[14] D. Benielli and J. Sommeria, Excitation of internal waves and stratified turbulence by parametric instability, Dyn. Atmos. Oceans **23**, 335 (1996).

[15] D. Benielli and J. Sommeria, Excitation and breaking of internal gravity waves by parametric instability, J. Fluid Mech. **374**, 117 (1998).

[16] S. Joubaud, J. Munroe, P. Odier, and T. Dauxois, Experimental parametric subharmonic instability in stratified fluids, Phys. Fluids **24**, 041703 (2012).

[17] P. J. Diamessis, S. Wunsch, I. Delwiche, and M. P. Richter, Nonlinear generation of harmonics through the interaction of an internal wave beam with a model oceanic pycnocline, Dyn. Atmos. Oceans **66**, 110 (2014).

[18] B. R. Sutherland, Excitation of superharmonics by internal modes in non-uniformly stratified fluid, J. Fluid Mech. **793**, 335 (2016).

[19] S. Wunsch, Harmonic generation by nonlinear self-interaction of a single internal wave mode, J. Fluid Mech. **828**, 630 (2017).

[20] D. Varma and M. Mathur, Internal wave resonant triads in finite-depth non-uniform stratifications, J. Fluid Mech. **824**, 286 (2017).
[21] W. R. Young, Y.-K. Tsang, and N. J. Balmforth, Near-inertial parametric subharmonic instability, J. Fluid Mech. **607**, 25 (2008).
[22] B. Bourget, T. Dauxois, S. Joubaud, and P. Odier, Experimental study of parametric subharmonic instability for internal plane waves, J. Fluid Mech. **723**, 1 (2013).
[23] L. Baker and B. R. Sutherland, The evolution of superharmonics excited by internal tides in non-uniform stratification, J. Fluid Mech. **891**, R1 (2020).
[24] T. S. van den Bremer, H. Yassin, and B. R. Sutherland, Lagrangian transport by vertically confined internal gravity wavepackets, J. Fluid Mech. **864**, 348 (2019).
[25] G. S. Carter and M. C. Gregg, Persistent near-diurnal internal waves observed above a site of M_2 barotropic-to-baroclinic conversion, J. Phys. Oceanogr. **36**, 1136 (2006).
[26] B. S. Chinn, J. B. Girton, and M. H. Alford, Observations of internal waves and parametric subharmonic instability in the Philippines archipelago, J. Geophys. Res. **117**, C05019 (2012).
[27] O. M. Sun and R. Pinkel, Subharmonic energy transfer from the semidiurnal internal time to near-diurnal motions over Kaena Ridge, Hawaii, J. Phys. Oceanogr. **43**, 766 (2013).
[28] R. Furue, Energy transfer within the small-scale oceanic internal wave spectrum, J. Phys. Oceanogr. **33**, 267 (2003).
[29] N. Furuichi, T. Habiya, and Y. Niwa, Bispectral analysis of energy transfer within the two-dimensional oceanic internal wave field, J. Phys. Oceanogr. **35**, 2104 (2005).